

1 **Relative contribution of atmospheric drivers to**
2 **‘extreme’ snowfall over the Amundsen Sea Embayment**

3 ¹ **Sai Prabala Swetha Chittella**

4 ² **Pranab Deb**

5 ^{1,2}Centre for Oceans, Rivers, Atmosphere and Land Sciences, Indian Institute of Technology Kharagpur

6 **Key Points:**

- 7 • The main drivers of extreme snowfall events over Amundsen Sea Embayment are
8 identified, and their relative contribution is quantified
9 • A coupled pattern consisting of Amundsen Sea low and a blocking high to the east is
10 the dominant driver of extreme snowfall during 1979-2016
11 • In addition, El Niño Southern Oscillation and ‘atmospheric rivers’ are also linked to
12 several extreme snowfall events over the region

Corresponding author: Pranab Deb, pranab@coral.iitkgp.ac.in

Abstract

We investigate the atmospheric drivers of extreme precipitation over the Amundsen Sea Embayment (ASE) of West Antarctica (WA) using daily output from RACMO2 model and reanalysis data (1979-2016). Empirical Orthogonal Function analysis of geopotential height anomalies (at 850 hPa) reveals that the dominant drivers of atmospheric variability over WA are the Southern Annular mode (SAM), PSA-patterns associated with Amundsen Sea low (ASL) and El Niño-Southern Oscillation (ENSO), and atmospheric rivers (ARs). Overall, 93.7% of days with extreme precipitation at the 2 coastal stations of ASE are associated with these patterns. ASL is the main driver of extreme precipitation over ASE (associated with 44.75% of extreme precipitation days) followed by PSA-1/ENSO (22.16%), ARs (21.1%) and SAM (12%). ASL is the main driver of extreme precipitation in all seasons except summer when ARs are dominant. Extreme precipitation linked to ASL and ARs are more intense (by ~ 2 mm/day) than the rest.

Plain Language Summary

Snowfall is a key component of the mass balance or ‘stability’ of the West Antarctic ice sheet. Around 41% of the total precipitation over the Amundsen Sea Embayment of West Antarctica comes from “extreme” snowfall events. We analyse the output from a regional climate model and global re-analysis data to study the seasonal distribution of these extreme events. We identify the atmospheric patterns responsible for these events, and quantify their relative importance. The low pressure system over Amundsen Sea was found to be the dominant driver of these events. Moreover, “atmospheric rivers” and remote forcing due to periodic warming of the tropical Pacific Ocean can also lead to extreme snowfall over the region.

1 Introduction

The contribution of Antarctic Ice Sheet to the global sea level rise has increased in recent decades, primarily due to ice loss driven by basal melting of ice shelves in West Antarctica (WA) and Antarctic Peninsula (H. Pritchard et al., 2012). The accumulated contribution of WA to sea level rise is 6.9 ± 0.6 mm since 1979 (Rignot et al., 2019). Warmer ocean temperature and incursions of warm circumpolar deep water onto the continental shelf are considered to be the key processes driving the basal melting of WA ice shelves (Vaughan et

43 al., 2001; Mayewski et al., 2009; Summerhayes et al., 2009; Turner et al., 2009; Bromwich
44 et al., 2013).

45
46 Antarctic Mass Balance is maintained by accumulation of precipitation, blowing snow and
47 ice loss due to melting, evaporation/sublimation and calving of ice along the coast. The
48 accelerated mass loss from the continent (Rignot et al., 2008; H. D. Pritchard et al., 2009)
49 is partially compensated by snowfall (Zwally et al., 2017; Paolo et al., 2018). As the atmo-
50 spheric moisture content over Antarctica is low, precipitation in coastal regions is mainly
51 dominated by intense ‘high’ precipitation events which are highly episodic, and driven
52 by moisture transport from low-latitude areas associated with certain synoptic conditions
53 (Noone & Simmonds, 1998; Sodemann & Stohl, 2009). Generally, these extreme precipita-
54 tion events (EPEs) are responsible for most of the annual precipitation over coastal Antarc-
55 tica (Turner et al., 2019). Turner et al. (2009) demonstrated that during 1979–2016, around
56 70% of the variance in annual precipitation of Antarctica is accounted for by variability in
57 EPEs, with the figure rising to 97% at one location over the Amundsen Sea Embayment
58 (ASE) (83°S , 146°W). Another recent study (MacLennan & Lenaerts, 2021) documents the
59 importance of EPEs over the Thwaites Glacier region in WA, with EPEs accounting for
60 around 60% of the total snowfall.

61
62 The spatial variability of different atmospheric and cryospheric parameters in WA is largely
63 controlled by the large-scale circulation patterns in the southern high latitudes, e.g., the
64 Southern Annular Mode (SAM), the Pacific-South American (PSA1 and PSA2) patterns
65 (Ghil & Mo, 1991; Lau et al., 1994; Kidson, 1988; Deb et al., 2016; G. J. Marshall et al.,
66 2017). The PSA1 pattern is known to be modulated by sea surface temperature anoma-
67 lies over tropical eastern Pacific Ocean i.e., ENSO variability (Mo & Paegle, 2001). ASE
68 has the strongest teleconnection to ENSO manifested via modifications in the Amundsen
69 Sea Low (ASL) (Deb et al., 2018). PSA2 is a dominant zonal wavenumber-3 pattern in
70 Southern Hemisphere which is also found to be influenced by tropical western Pacific Ocean
71 (M. Raphael, 2004; Clem & Fogt, 2015, 2015; Irving & Simmonds, 2015). A coupled at-
72 mospheric structure consisting of a blocking high to the west of Antarctic Peninsula and
73 the ASL represents the western branch of the PSA2 pattern (M. Raphael, 2004), and drives
74 a strong meridional flow towards the coastal WA (Deb et al., 2018). G. J. Marshall et al.
75 (2017) showed that polarities of these principal modes of atmospheric circulation control

76 the EPEs over Antarctica. Moreover, “atmospheric rivers” that carry copious amount of
77 moisture from midlatitudes have also been linked to several coastal EPEs in Antarctica (Zhu
78 & Newell, 1998; Gorodetskaya et al., 2014).

79
80 The scarceness and uneven distribution of observation records limit our understanding of
81 the fine scale distribution of precipitation, particularly over the coastal regions (Banta et al.,
82 2008; Maclennan & Lenaerts, 2021). Moreover reanalyses products and global climate model
83 simulations are too coarse to capture the complex spatial pattern of topography and related
84 meteorological processes over the region (Orr et al., 2014; Deb et al., 2016). To this end,
85 dynamical downscaling of global reanalysis data using limited-area high-resolution regional
86 atmospheric models (e.g., Giorgi et al. (1994)) has emerged as a useful tool to generate
87 physically consistent temporal and spatial pattern of Antarctic precipitation (J. T. Lenaerts
88 et al., 2013; G. J. Marshall et al., 2017). For example, the performance of the Regional
89 Atmospheric Climate Model (RACMO) has been vetted by two recent studies in captur-
90 ing the mean and extreme precipitation over Antarctica (Turner et al., 2019; Maclennan
91 & Lenaerts, 2021). These studies have attempted to quantify the variability and contribu-
92 tion of extreme snowfall events over Antarctica (Turner et al., 2019), and to identify the
93 atmospheric drivers of EPEs over the Thwaites glacier region of WA (e.g., Thwaites glacier).

94
95 However, no studies exist that quantify the role of dominant atmospheric drivers of EPEs
96 across the ASE, or quantify the seasonal contribution of these drivers to the occurrence of
97 EPEs. Here, we present the intensity and frequency of EPEs over ASE using output from
98 a high-resolution regional climate model (RACMO2). Thereafter, we identify the primary
99 atmospheric drivers of these EPEs, and quantify their relative and seasonal contribution.

100 **2 Data and methods**

101 Daily precipitation flux derived from an Antarctic-wide simulation of RACMO2 (version
102 2.3, Van Wessem et al. (2014)) during the period from 1979-2016 (January to December) is
103 used to calculate daily precipitation (mm/day). The model uses a horizontal resolution of
104 27 km and a vertical resolution of 40 levels. The model combines the atmospheric dynam-
105 ics of the High Resolution Limited Area Model (HIRLAM; Undén et al. (2002)) with the
106 physics package of the European Centre for Medium-Range Weather Forecasts (ECMWF)
107 Integrated Forecast System (IFS). The model is forced by 6-hourly ERA-Interim reanalysis

108 data (Dee et al., 2011), and the interior of domain is set free while the lateral and ocean
109 boundaries are constrained. This model version 2.3 is optimised for polar regions by inter-
110 actively coupling it to a multilayer snow model (Ettema et al., 2010). A prognostic scheme
111 for snow grain size is used for the calculation of snow albedo (Kuipers Munneke et al., 2011)
112 while the interaction of the near-surface air with drifting snow is simulated by drifting snow
113 scheme (Déry & Yau, 1999; J. Lenaerts et al., 2010).

114

115 We define daily EPEs as days during which daily precipitation exceeds the 95th percentile of
116 daily precipitation values of the whole time series. Empirical Orthogonal Function (EOF)
117 analysis of daily geopotential height anomaly was performed to identify the dominant pat-
118 terns of atmospheric variability over WA. Spatial patterns of the major EOF modes over
119 the domain encompassing 60°-90°S and 180°-60°W were computed by considering the daily
120 geopotential height anomalies at 850 hPa derived from ERA-Interim re-analysis at a hori-
121 zontal resolution of 0.75° by 0.75° during 1979-2016. The time series of these EOF modes
122 are called principal components (PCs), are normalised such that their mean is zero and
123 standard deviation is one. Next, the values of the normalised major PCs are extracted for
124 each EPE day. For a particular EPE day, a PC mode is considered to be dominant if the
125 magnitude of the normalised PC is greater than 1 for that day.

126

127 Further, moisture divergence and moisture transport data derived from ERA-Interim re-
128 analysis were used to study the atmospheric condition during EPE days. To identify the
129 climatic drivers of the EPEs, several global climate indices were also analysed, e.g., ENSO
130 (National Weather Service Climate Prediction Center), Marshall SAM index (G. Marshall,
131 2018), ASL index (S. Hosking, 2020). We also define an ASL-lon index, following Deb et al.
132 (2018), as the difference between mean sea level pressure averaged over a box in the western
133 Amundsen Sea region (to the west of 125°W; labeled “Box 1” in Figure-1a) and a box in
134 the Bellingshausen Sea (to the east of 110°W, labeled “Box 2” in Figure-1a). Positive (neg-
135 ative) values of index indicates the eastward (westward) shift of the location of the ASL.
136 This index effectively captures the blocking pattern over WA and the zonal migration of
137 ASL.

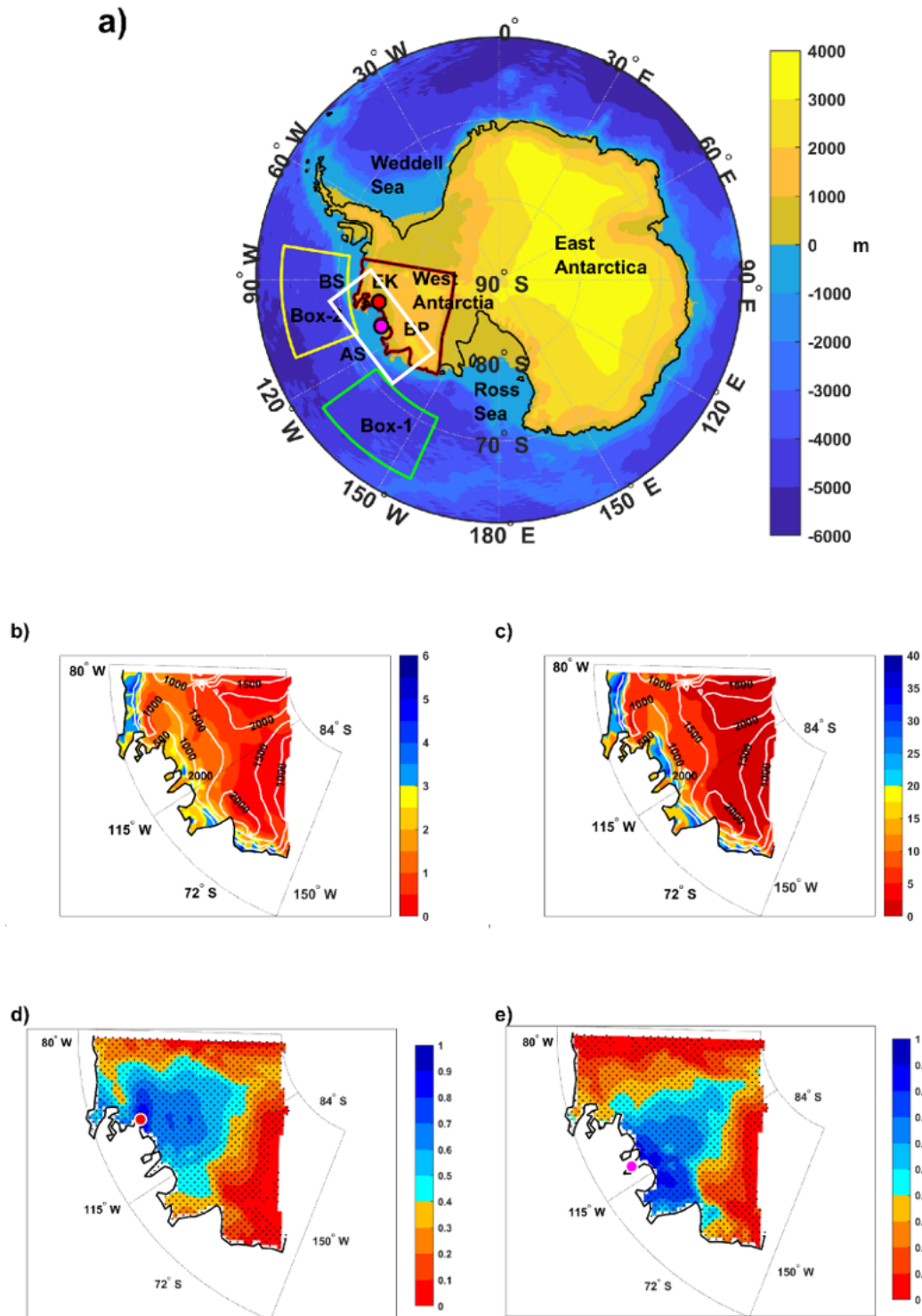


Figure 1. (a) Map of Antarctica with surface elevation in the background (shaded, in m). The Study area outlined in thick red lines. White box is the region of Amundsen Sea Embayment. EK-Evans Knoll, BP-Bear Peninsula, BS- Bellingshausen sea, AS-Amundsen sea, box-1 and box-2 are regions in AS and BS. Spatial distribution of (b) average daily precipitation (mm/day) and (c) average precipitation (mm/day) from all EPEs at each grid of study area for time period 1979-2016. Correlation between (d) Evans Knoll and (e) Bear Peninsula to study domain at 95% significant level.

3 Results

Spatial distribution of average daily precipitation over WA during 1979-2016 is shown in Figure-1b. Coastal areas with elevation less than 1000 m are associated with higher average precipitation values (> 3 mm/day). The average precipitation values drop down to below 2 mm/day in the inland areas. Over the coastal areas, the mean daily precipitation from EPEs (Figure-1c) is approximately 7 times more than that of average daily precipitation (Figure-1b). The mean precipitation from EPEs is much lower (< 10 mm/day) when compared to coastal areas. Overall, the total precipitation accumulated for the whole domain (outlined in thick red lines in Figure-1a) is 1.9471×10^4 Gt out of which the total contribution from EPEs is 6.8523×10^3 Gt during 1979-2016. Thus, EPEs contribute 35.19% to the total precipitation over the WA domain.

In coastal areas, the mean precipitation linked to EPEs show large values, particularly over the ASE region. In order to capture the characteristics and drivers of EPEs over the ASE, two coastal locations, namely Evans Knoll (EK, red circle in Figure-1d) and Bear Peninsula (BP, magenta circle in Figure-1e), are selected. Interestingly, time series of average daily precipitation from the two stations are closely related to one another (correlation of 0.7). Moreover, the daily average precipitation at these two stations are significantly correlated to a large portion of the WA, with particularly high correlation over the ASE (Figures-1d and 1e). The precipitation over EK shows the strongest correlation with precipitation over ASE to the east of 115°W (correlation > 0.6), while the precipitation over BP is strongly associated with precipitation over ASE to the west of 95°W (correlation > 0.6). Since, the precipitation at these two locations are representative of precipitation over the entire ASE (and also over a larger WA domain), we focus on these locations instead of area averaged values over ASE.

The frequency distribution and seasonality of EPEs are similar at both the locations with the maximum number of EPEs occurring in JJA, followed by MAM and SON. Significantly less number of EPEs are found in DJF (Supplementary Figure-S1 and S2). Given the strong correlation with precipitation over the rest of the domain, a similar frequency distribution and seasonal variability is expected over most of the WA domain. The rest of this section will focus on identifying the key drivers of EPEs at the two locations.

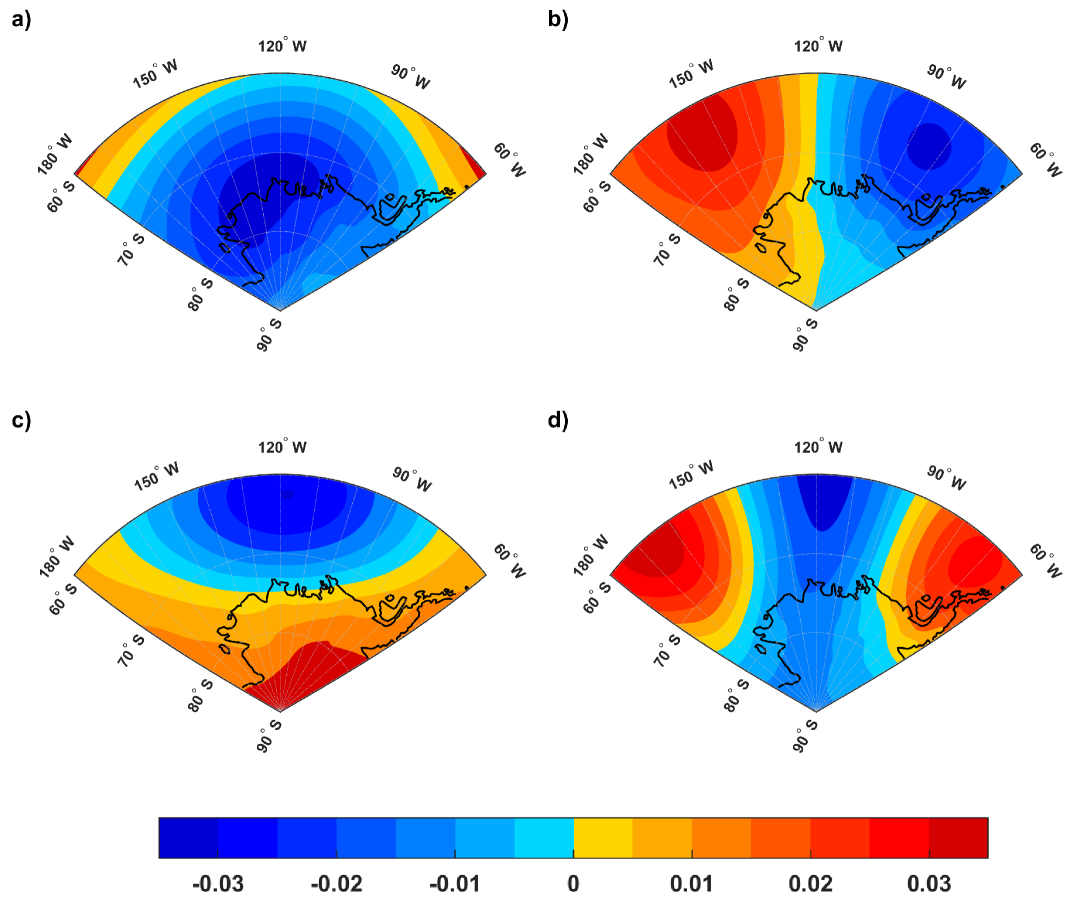


Figure 2. Spatial analysis of first four EOF modes (a,b,c and d) of geopotential height at 850 hpa over the region 60° S to 90° S and 180° W to 60° W.

3.1 Dominant patterns of atmospheric variability over coastal WA

The dominant modes of near-surface atmospheric circulation over the study domain are identified from the EOF analysis of daily geopotential height anomalies at 850 hPa. The first dominant mode (EOF-1) which explains $\sim 48\%$ of the total variability is the Southern Annular Mode (SAM, Limpasuvan and Hartmann (1999); Thompson and Wallace (2000)). The spatial pattern is associated with an annular structure and a negative anomaly centred at 130°W (Figure-2a). The first PC time series shows a strong positive correlation (> 0.7) with SAM and it has a weak negative correlation with ASL- actual central pressure index (Supplementary Table S1).

The second EOF mode (EOF-2) (Figure-2b) explains $\sim 19\%$ variability. The spatial pattern is characterised by positive anomalies centred at 150°W (Amundsen Sea region in the western WA) and negative anomalies centred at 90°W (west of Antarctic Peninsula). This spatial pattern, consisting of pressure anomalies of opposite signs to the west of Antarctic Peninsula and over the Amundsen Sea region, is representative of the western branch of the PSA2 pattern. The change in polarity of this pattern (equivalent to a zonal shift in ASL) can be conveniently represented by the ASL lon index as presented in Deb et al. (2018). This is evident from a strong positive correlation (> 0.9) of the corresponding PC with ASL-lon index (Table S1).

The spatial pattern of EOF-3 mode (Figure-2c), which accounts for $\sim 17.14\%$ of total variability, resembles the ENSO spatial pattern with negative (positive) anomalies over Amundsen Sea during El Niño (La Niña) events (Clem & Fogt, 2013; Deb et al., 2018). The modulation of this mode by eastern Pacific Ocean is further evident from a significant negative correlation (~ -0.5) of the PC time series with ENSO index (Table S1).

The EOF-4 mode explains around 8.04% of the total variability, and resembles the structure of an ‘atmospheric river’ consisting of an elongated negative anomaly pattern extending from mid latitudes onto the continent (Figure-2d). The pattern, along with the blocking structures on either sides, shows close proximity to the observed atmospheric river pattern mentioned in Wille et al. (2019).

The following subsection will focus on the contribution of these atmospheric modes towards moisture convergence and precipitation over the two stations over the ASE.

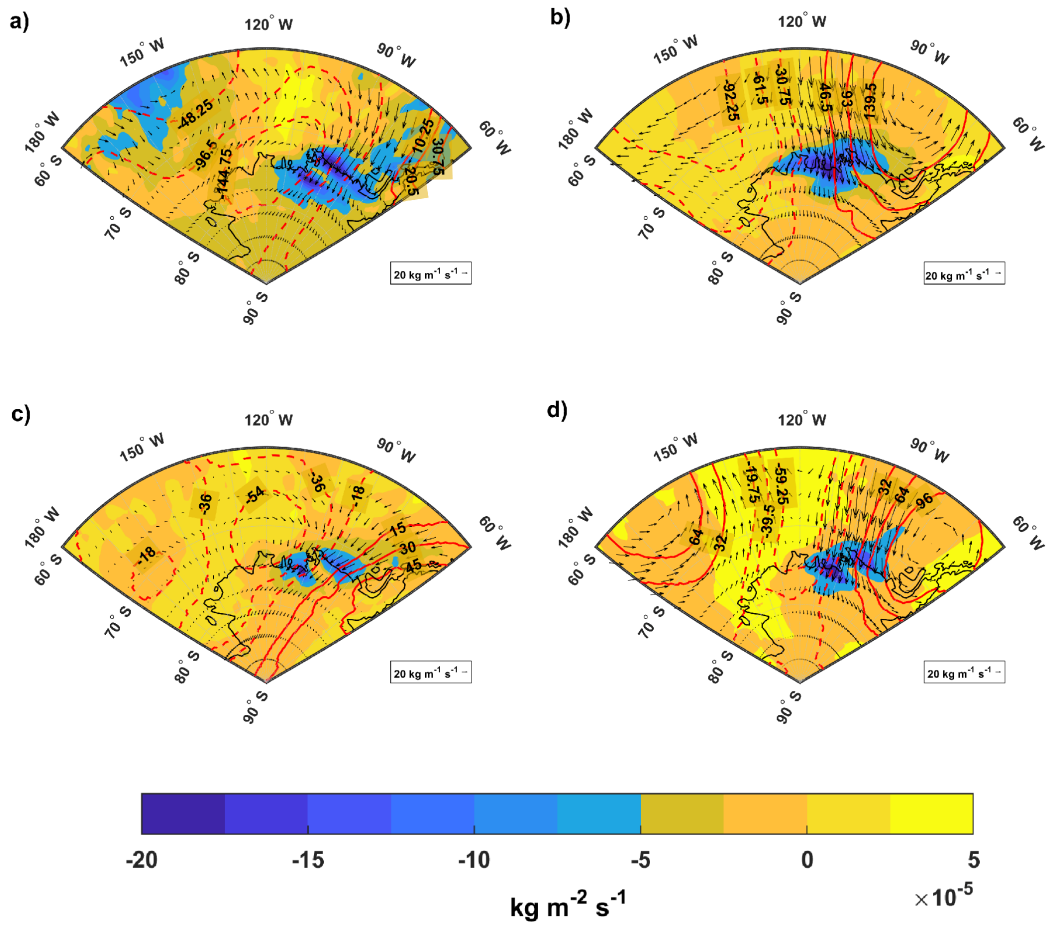


Figure 3. Composite anomalies of moisture divergence (shaded, in $\text{kg m}^{-2} \text{s}^{-1}$), moisture transport (vectors, in $\text{kg m}^{-1} \text{s}^{-1}$) and geopotential height at 850 hpa (positive and negative anomalies are represented by red solid lines and red dotted contours, respectively) during EPE days of EK, when only respective PC-1 (a), PC-2 (b), PC-3 (c) and PC-4 (d) modes are dominant.

203 **3.2 Role of the main atmospheric modes in driving EPEs over coastal WA**

204 A particular atmospheric mode is considered to play the dominant role during an EPE day
 205 if the corresponding PC on that day shows the largest value among the 4 major modes.
 206 Composites of 3 important variables (e.g., divergence of moisture flux, moisture transport
 207 and geopotential height anomalies at 850 hPa) are computed during EPE days at EK dom-
 208 inated by each individual mode (Figure-3). For example, Figure-3a shows the composite
 209 for EPE days dominated by the first EOF mode. A cyclonic geopotential height anomaly
 210 is noticed over coastal WA which is consistent with the spatial pattern of EOF-1 mode in
 211 Figure-2a. A strong meridional moisture transport towards the continent leads to intense
 212 moisture convergence (magnitude $> 5 \cdot 10^{-5} \text{ kgm}^{-2}\text{s}^{-1}$) along the eastern WA coastline (be-
 213 tween 120°W and 60°W) and western Antarctic Peninsula (blue shading). This circulation
 214 anomaly explains the occurrence of EPEs at EK station during the days dominated by first
 215 mode of atmospheric variability over WA, i.e., the SAM. Figure-3b shows that the EPE
 216 days at EK that are dominated by the second EOF mode show a dipole-like geopotential
 217 anomaly pattern with anti-cyclonic and cyclonic anomaly centres to the east (west) of \sim
 218 110°W . This pattern (which is clearly similar to spatial pattern of the second EOF mode)
 219 drives a strong meridional moisture transport towards the WA coast, with the strongest
 220 moisture convergence (magnitude $> 5 \cdot 10^{-5} \text{ kg/m/s}$) concentrated over the ASE ($140^\circ\text{W} -$
 221 90°W). Atmospheric circulation pattern during EPE days (at EK) dominated by the third
 222 EOF mode is shown in Figure-3c. Similar to the spatial pattern of EOF-3 (as shown in
 223 Figure-2c), a cyclonic circulation anomaly is observed over the Amundsen Sea region ac-
 224 companied by anomalous moisture transport towards the coastal WA leading to intense
 225 moisture convergence along the coastline. However, the area of the strongest moisture con-
 226 vergence (i.e., magnitude $> 5 \cdot 10^{-5} \text{ kgm}^{-2}\text{s}^{-1}$) is limited within the ASE (e.g., $100^\circ\text{W} -$
 227 80°W longitude belt). Therefore, the cyclonic circulation anomaly associated with the third
 228 mode can bring copious amount of moisture towards the coastal stations over the ASE and
 229 cause EPEs.

230
 231 EPE days at EK that are dominated by EOF-4 mode show a distinct atmospheric river
 232 pattern (Figure-3d). This pattern is associated with strong moisture transport towards the
 233 coastal WA and leads to intense moisture convergence with particularly large values (mag-
 234 nitude $> 5 \cdot 10^{-5} \text{ kgm}^{-2}\text{s}^{-1}$) concentrated over the ASE ($110^\circ\text{W} - 80^\circ\text{W}$ longitude belt).
 235 Similarly, the composite anomalies during EPE days at BP when dominated by 4 individ-

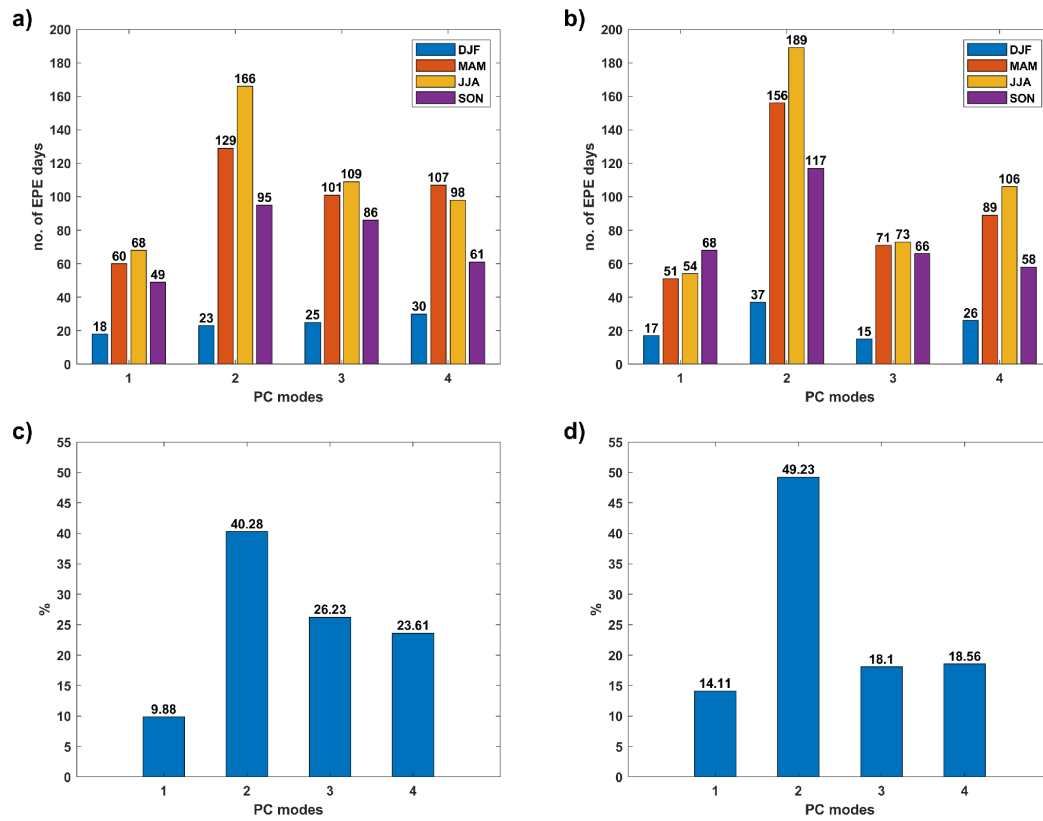


Figure 4. Seasonal distribution of EPE days and PCs of (a) EK and (b) BP. Percentage contribution of dominant PCs to EPEs of (c) EK and (d) BP.

236 ual EOF modes are shown in Supplementary figure-S3. The composite anomaly patterns
237 remain broadly similar to that in the case of EK (i.e., Figure-3). However, the spatial ex-
238 tent of moisture convergence is less when compared to that of EK (Figure-3) but is found
239 to be more intense near coastal ASE region. Supplementary figure-S3 is same as Figure-3
240 but shows the composites of only precipitation anomalies over the WA domain. It is clear
241 that the magnitude of precipitation associated with ASL-lon and AR is larger by at least 2
242 mm/day.

243 **3.3 Relative seasonal contribution of different atmospheric modes**

244 Figure-4a and b indicates the seasonal contribution of EOFs to EPEs at the two coastal
245 locations over WA while the ‘total’ contribution of the EOF modes is shown in Figure-4c
246 and d. The second EOF mode or the ASL-lon zonal pattern (i.e., the coupling of ASL
247 with a blocking high over the Antarctic Peninsula) was found to be the leading driver of
248 EPEs over coastal WA with a total contribution of 40.28% (49.23 %) at EK (BP) (Figure-
249 4c and 4d). This pattern was previously reported to be the main driver of high snowfall
250 events over Thwaites Glacier region of WA (Maclennan & Lenaerts, 2021). The pattern is
251 particularly important for EPEs during MAM, JJA and SON seasons (Figure-4a and 4b).
252 This is followed by EOF-3 (representative of ENSO influence over WA) and EOF-4 (linked
253 to the intrusion of atmospheric rivers) modes with percentage contributions of 26.23 and
254 23.61, respectively, to EPE days at EK (Figure-4c). Their respective contribution is 18.1 %
255 and 18.56 % at BP (Figure-4d). On average, EOF-4 is slightly more dominant than EOF-3
256 during DJF, MAM and JJA seasons while EOF-3 is more dominant in SON (Figure-4a and
257 4b). In contrast, the first EOF mode associated with SAM showed the least percentage
258 contribution to EPE days in all four seasons. The total contribution of EOF-1 to EPE days
259 is 9.88 % and 14.11 % at EK and BP, respectively.

260 **4 Discussion and Conclusions**

261 Despite several attempts to understand the seasonal and inter annual changes in mass bal-
262 ance and precipitation over WA, only a few studies have attempted to understand the short
263 lived extreme precipitation events and their atmospheric drivers. Most of annual precipita-
264 tion over the coastal WA comes from EPEs (Turner et al., 2019). For example, we find that
265 at two coastal stations over the ASE of WA (EK and BP), EPEs contribute around 41% of
266 the total precipitation, with the maximum contribution from EPEs noted in winter followed

267 by autumn, spring and summer seasons. As EK and BP are representative of the precipita-
268 tion over the coastal WA, and also over inland areas (as evident from the significantly high
269 correlation in Figure-1a), precipitation from these two stations are used to understand the
270 frequency distribution and drivers of EPEs over coastal WA, and particularly the ASE.

271
272 The ‘ASL-lon’ pattern or the zonally coupled structure consisting of ASL and a block-
273 ing high over the Antarctic Peninsula was found to be the leading driver of EPEs over the
274 ASE. Total contribution from ‘ASL-lon’ pattern to EPEs at the coastal stations over the
275 ASE ($\sim 40 - 49\%$) is significantly higher than the total contribution from PSA-1 pattern
276 ($\sim 18 - 26\%$) and the atmospheric river pattern ($\sim 18 - 23\%$). The ‘ASL-lon’ pattern
277 was previously shown to be responsible for high snowfall events over Thwaites Glacier re-
278 gion of WA in a previous study (MacLennan & Lenaerts, 2021). ASL-lon pattern shows
279 the maximum (minimum) contribution to EPEs in winter (summer). This seasonality in the
280 contribution of ASL-lon is due to the well-defined annual cycle in the zonal location of
281 ASL with a clear westward movement towards the Ross Sea in winter which drives strong
282 northerly wind into the ASE (J. S. Hosking et al., 2013; M. N. Raphael et al., 2016).

283
284 El Niño years associated with a large positive geopotential height anomaly centre off the
285 coast of WA which drives anomalous warm and moist air advection into the WA ice sheet
286 (Welhouse et al., 2016; Deb et al., 2018). The local circulation changes during El Niño
287 years are associated with an increased likelihood of extreme surface temperature (Deb et
288 al., 2018), and an increase in precipitation over the ASE (Paolo et al., 2018; Zhang et al.,
289 2021). The ENSO signal over WA is captured by EOF-3 mode in our study, and explains
290 more than 25% of the EPEs over coastal WA.

291
292 AR pattern is represented by EOF-4 mode in our analysis and explains only 8% of the
293 total variability, but it is associated with the most intense moisture convergence among all
294 the modes (Figure-4). Despite their extreme rarity, ARs have been linked to a number of
295 heavy precipitation events across Antarctica (Gorodetskaya et al., 2014; Wille et al., 2019;
296 Adusumilli et al., 2021). Our analysis shows that during the simulation period of 1979-
297 2016, ARs are associated with approximately 18-24% of the extreme snowfall days over
298 ASE. However, their contribution in terms of the actual amount of snowfall will be much
299 higher as the EPEs during ARs are much more intense (Supplementary figure-S4) due to

300 the high moisture convergence.

301
302 As a large fraction (around 35%) of the precipitation over coastal WA comes from EPEs,
303 the future mass balance changes over WA will be highly sensitive to the future changes in
304 the atmospheric drivers of EPEs identified in this study. A westward (and poleward) shift
305 of ASL (J. S. Hosking et al., 2016; Brown et al., 2020) along with a likely increase in the
306 frequency of ARs land falling on Antarctica by the end of the 21st century (Espinoza et
307 al., 2018; Payne et al., 2021) are expected to make a positive contribution to future mass
308 balance changes over WA. However, projected change in ENSO, and hence the associated
309 teleconnection, remain highly uncertain. Therefore, it is essential that the dynamics of these
310 drivers and their interaction with the WA coastline are well-understood in order to constrain
311 the future mass balance changes over ASE and coastal WA.

312 **5 Open Research**

313 The data required to reproduce the above findings are available to download from
314 [https://ramadda.data.bas.ac.uk/repository/entry/show?entryid=bbf12a6f-7d97-4951](https://ramadda.data.bas.ac.uk/repository/entry/show?entryid=bbf12a6f-7d97-4951-9bd1-e4224e2abac9)
315 [-9bd1-e4224e2abac9](https://ramadda.data.bas.ac.uk/repository/entry/show?entryid=bbf12a6f-7d97-4951-9bd1-e4224e2abac9),
316 <https://apps.ecmwf.int/datasets/>,
317 <https://climatedataguide.ucar.edu/climate-data/amundsen-sea-low-indices>,
318 [https://climatedataguide.ucar.edu/climate-data/marshall-southern-annular-mode](https://climatedataguide.ucar.edu/climate-data/marshall-southern-annular-mode-sam-index-station-based)
319 [-sam-index-station-based](https://climatedataguide.ucar.edu/climate-data/marshall-southern-annular-mode-sam-index-station-based),
320 [https://origin.cpc.ncep.noaa.gov/products/analysis_monitoring/ensostuff/ONI.v5](https://origin.cpc.ncep.noaa.gov/products/analysis_monitoring/ensostuff/ONI.v5.php)
321 [.php](https://origin.cpc.ncep.noaa.gov/products/analysis_monitoring/ensostuff/ONI.v5.php)

322 **Acknowledgments**

323 Both the authors were funded by the Indian Institute of Technology Kharagpur and the
324 Ministry of Education, Govt. of India. We also acknowledge the support of the National
325 Centre for Polar and Ocean Research, Goa (project: NCPOR/2019/PACER-POP/AS-02).

326 **References**

327 Adusumilli, S., A Fish, M., Fricker, H. A., & Medley, B. (2021). Atmospheric river precipi-
328 tation contributed to rapid increases in surface height of the west antarctic ice sheet
329 in 2019. *Geophysical Research Letters*, 48(5), e2020GL091076.

- 330 Banta, J. R., McConnell, J. R., Frey, M. M., Bales, R. C., & Taylor, K. (2008). Spatial and
331 temporal variability in snow accumulation at the west antarctic ice sheet divide over
332 recent centuries. *Journal of Geophysical Research: Atmospheres*, *113*(D23).
- 333 Bromwich, D. H., Nicolas, J. P., Monaghan, A. J., Lazzara, M. A., Keller, L. M., Weidner,
334 G. A., & Wilson, A. B. (2013). Central west antarctica among the most rapidly
335 warming regions on earth. *Nature Geoscience*, *6*(2), 139–145.
- 336 Brown, J. R., Brierley, C. M., An, S.-I., Guarino, M.-V., Stevenson, S., Williams, C. J., ...
337 others (2020). Comparison of past and future simulations of enso in cmip5/pmip3
338 and cmip6/pmip4 models. *Climate of the Past*, *16*(5), 1777–1805.
- 339 Clem, K. R., & Fogt, R. L. (2013). Varying roles of enso and sam on the antarctic peninsula
340 climate in austral spring. *Journal of Geophysical Research: Atmospheres*, *118*(20),
341 11–481.
- 342 Clem, K. R., & Fogt, R. L. (2015). South pacific circulation changes and their connection
343 to the tropics and regional antarctic warming in austral spring, 1979–2012. *Journal*
344 *of Geophysical Research: Atmospheres*, *120*(7), 2773–2792.
- 345 Deb, P., Orr, A., Bromwich, D. H., Nicolas, J. P., Turner, J., & Hosking, J. S. (2018).
346 Summer drivers of atmospheric variability affecting ice shelf thinning in the amundsen
347 sea embayment, west antarctica. *Geophysical Research Letters*, *45*(9), 4124–4133.
- 348 Deb, P., Orr, A., Hosking, J. S., Phillips, T., Turner, J., Bannister, D., ... Colwell, S.
349 (2016). An assessment of the polar weather research and forecasting (wrf) model
350 representation of near-surface meteorological variables over west antarctica. *Journal*
351 *of Geophysical Research: Atmospheres*, *121*(4), 1532–1548.
- 352 Dee, D. P., Uppala, S. M., Simmons, A. J., Berrisford, P., Poli, P., Kobayashi, S., ...
353 others (2011). The era-interim reanalysis: Configuration and performance of the data
354 assimilation system. *Quarterly Journal of the royal meteorological society*, *137*(656),
355 553–597.
- 356 Déry, S. J., & Yau, M. (1999). A bulk blowing snow model. *Boundary-Layer Meteorology*,
357 *93*(2), 237–251.
- 358 Espinoza, V., Waliser, D. E., Guan, B., Lavers, D. A., & Ralph, F. M. (2018). Global anal-
359 ysis of climate change projection effects on atmospheric rivers. *Geophysical Research*
360 *Letters*, *45*(9), 4299–4308.
- 361 Ettema, J., Van den Broeke, M., Van Meijgaard, E., Van de Berg, W., Box, J., & Steffen, K.
362 (2010). Climate of the greenland ice sheet using a high-resolution climate model—part

- 363 1: Evaluation. *The Cryosphere*, 4(4), 511–527.
- 364 Ghil, M., & Mo, K. (1991). Intraseasonal oscillations in the global atmosphere. part ii:
365 Southern hemisphere. *Journal of Atmospheric Sciences*, 48(5), 780–790.
- 366 Giorgi, F., Shields Brodeur, C., & Bates, G. T. (1994). Regional climate change scenarios
367 over the united states produced with a nested regional climate model. *Journal of*
368 *Climate*, 7(3), 375–399.
- 369 Gorodetskaya, I. V., Tsukernik, M., Claes, K., Ralph, M. F., Neff, W. D., & Van Lipzig,
370 N. P. (2014). The role of atmospheric rivers in anomalous snow accumulation in east
371 antarctica. *Geophysical Research Letters*, 41(17), 6199–6206.
- 372 Hosking, J. S., Orr, A., Bracegirdle, T. J., & Turner, J. (2016). Future circulation changes
373 off west antarctica: Sensitivity of the amundsen sea low to projected anthropogenic
374 forcing. *Geophysical Research Letters*, 43(1), 367–376.
- 375 Hosking, J. S., Orr, A., Marshall, G. J., Turner, J., & Phillips, T. (2013). The influence
376 of the amundsen–bellingshausen seas low on the climate of west antarctica and its
377 representation in coupled climate model simulations. *Journal of Climate*, 26(17),
378 6633–6648.
- 379 Hosking, S. (2020). *The climate data guide: Amundsen sea low indices*, edited by: National
380 center for atmospheric research staff. Retrieved from [https://climatedataguide](https://climatedataguide.ucar.edu/climate-data/amundsen-sea-low-indices)
381 [.ucar.edu/climate-data/amundsen-sea-low-indices](https://climatedataguide.ucar.edu/climate-data/amundsen-sea-low-indices)
- 382 Irving, D., & Simmonds, I. (2015). A novel approach to diagnosing southern hemisphere
383 planetary wave activity and its influence on regional climate variability. *Journal of*
384 *Climate*, 28(23), 9041–9057.
- 385 Kidson, J. W. (1988). Interannual variations in the southern hemisphere circulation. *Journal*
386 *of Climate*, 1(12), 1177–1198.
- 387 Kuipers Munneke, P., Van den Broeke, M., Lenaerts, J., Flanner, M., Gardner, A., & Van de
388 Berg, W. (2011). A new albedo parameterization for use in climate models over the
389 antarctic ice sheet. *Journal of Geophysical Research: Atmospheres*, 116(D5).
- 390 Lau, K., Sheu, P., & Kang, I.-S. (1994). Multiscale low-frequency circulation modes in the
391 global atmosphere. *Journal of the Atmospheric Sciences*, 51(9), 1169–1193.
- 392 Lenaerts, J., Van den Broeke, M., Déry, S., König-Langlo, G., Ettema, J., & Munneke, P. K.
393 (2010). Modelling snowdrift sublimation on an antarctic ice shelf. *The Cryosphere*,
394 4(2), 179–190.
- 395 Lenaerts, J. T., van Meijgaard, E., van den Broeke, M. R., Ligtenberg, S. R., Horwath, M., &

- 396 Isaksson, E. (2013). Recent snowfall anomalies in dronning maud land, east antarctica,
397 in a historical and future climate perspective. *Geophysical Research Letters*, *40*(11),
398 2684–2688.
- 399 Limpasuvan, V., & Hartmann, D. L. (1999). Eddies and the annular modes of climate
400 variability. *Geophysical Research Letters*, *26*(20), 3133–3136.
- 401 MacLennan, M. L., & Lenaerts, J. T. (2021). Large-scale atmospheric drivers of snowfall over
402 thwaites glacier, antarctica. *Geophysical Research Letters*, *48*(17), e2021GL093644.
- 403 Marshall, G. (2018). *The climate data guide: Marshall southern annular mode (sam) index*
404 *(station-based)*, edited by: National center for atmospheric research staff.
- 405 Marshall, G. J., Thompson, D. W., & van den Broeke, M. R. (2017). The signature
406 of southern hemisphere atmospheric circulation patterns in antarctic precipitation.
407 *Geophysical Research Letters*, *44*(22), 11–580.
- 408 Mayewski, P. A., Meredith, M., Summerhayes, C., Turner, J., Worby, A., Barrett, P., ...
409 others (2009). State of the antarctic and southern ocean climate system. *Reviews of*
410 *Geophysics*, *47*(1).
- 411 Mo, K. C., & Paegle, J. N. (2001). The pacific–south american modes and their downstream
412 effects. *International Journal of Climatology: A Journal of the Royal Meteorological*
413 *Society*, *21*(10), 1211–1229.
- 414 Noone, D., & Simmonds, I. (1998). Implications for the interpretation of ice-core isotope
415 data from analysis of modelled antarctic precipitation. *Annals of Glaciology*, *27*,
416 398–402.
- 417 Orr, A., Phillips, T., Webster, S., Elvidge, A., Weeks, M., Hosking, S., & Turner, J. (2014).
418 Met office unified model high-resolution simulations of a strong wind event in antarctica.
419 *Quarterly Journal of the Royal Meteorological Society*, *140*(684), 2287–2297.
- 420 Paolo, F., Padman, L., Fricker, H., Adusumilli, S., Howard, S., & Siegfried, M. (2018).
421 Response of pacific-sector antarctic ice shelves to the el niño/southern oscillation.
422 *Nature geoscience*, *11*(2), 121–126.
- 423 Payne, A. J., Nowicki, S., Abe-Ouchi, A., Agosta, C., Alexander, P., Albrecht, T., ... others
424 (2021). Future sea level change under coupled model intercomparison project phase
425 5 and phase 6 scenarios from the greenland and antarctic ice sheets. *Geophysical*
426 *Research Letters*, *48*(16), e2020GL091741.
- 427 Pritchard, H., Ligtenberg, S. R., Fricker, H. A., Vaughan, D. G., van den Broeke, M. R.,
428 & Padman, L. (2012). Antarctic ice-sheet loss driven by basal melting of ice shelves.

- 429 *Nature*, *484*(7395), 502–505.
- 430 Pritchard, H. D., Arthern, R. J., Vaughan, D. G., & Edwards, L. A. (2009). Extensive
431 dynamic thinning on the margins of the greenland and antarctic ice sheets. *Nature*,
432 *461*(7266), 971–975.
- 433 Raphael, M. (2004). A zonal wave 3 index for the southern hemisphere. *Geophysical*
434 *Research Letters*, *31*(23).
- 435 Raphael, M. N., Marshall, G., Turner, J., Fogt, R., Schneider, D., Dixon, D., ... Hobbs,
436 W. R. (2016). The amundsen sea low: variability, change, and impact on antarctic
437 climate. *Bulletin of the American Meteorological Society*, *97*(1), 111–121.
- 438 Rignot, E., Bamber, J. L., Van Den Broeke, M. R., Davis, C., Li, Y., Van De Berg, W. J.,
439 & Van Meijgaard, E. (2008). Recent antarctic ice mass loss from radar interferometry
440 and regional climate modelling. *Nature geoscience*, *1*(2), 106–110.
- 441 Rignot, E., Mouginot, J., Scheuchl, B., Van Den Broeke, M., Van Wessem, M. J., &
442 Morlighem, M. (2019). Four decades of antarctic ice sheet mass balance from 1979–
443 2017. *Proceedings of the National Academy of Sciences*, *116*(4), 1095–1103.
- 444 Sodemann, H., & Stohl, A. (2009). Asymmetries in the moisture origin of antarctic precip-
445 itation. *Geophysical research letters*, *36*(22).
- 446 Summerhayes, C., Ainley, D., Barrett, P., Bindschadler, R., Clarke, A., Convey, P., ...
447 others (2009). The antarctic environment in the global system. *Antarctic climate*
448 *change and the environment. Scientific Committee on Antarctic Research, Cambridge*,
449 1–32.
- 450 Thompson, D. W., & Wallace, J. M. (2000). Annular modes in the extratropical circulation.
451 part i: Month-to-month variability. *Journal of climate*, *13*(5), 1000–1016.
- 452 Turner, J., Bindschadler, R., Convey, P., Di Prisco, G., Fahrbach, E., Gutt, J., ... Sum-
453 merhayes, C. (2009). *Antarctic climate change and the environment*.
- 454 Turner, J., Phillips, T., Thamban, M., Rahaman, W., Marshall, G. J., Wille, J. D., ...
455 others (2019). The dominant role of extreme precipitation events in antarctic snowfall
456 variability. *Geophysical Research Letters*, *46*(6), 3502–3511.
- 457 Undén, P., Rontu, L., Järvinen, H., Lynch, P., Calvo, J., Cats, G., ... others (2002).
458 Hirlam-5 scientific documentation.
- 459 Van Wessem, J., Reijmer, C., Morlighem, M., Mouginot, J., Rignot, E., Medley, B., ...
460 others (2014). Improved representation of east antarctic surface mass balance in a
461 regional atmospheric climate model. *Journal of Glaciology*, *60*(222), 761–770.

- 462 Vaughan, D. G., Marshall, G. J., Connolley, W. M., King, J. C., & Mulvaney, R. (2001).
463 Devil in the detail. *Science*, *293*(5536), 1777–1779.
- 464 Welhouse, L. J., Lazzara, M. A., Keller, L. M., Tripoli, G. J., & Hitchman, M. H. (2016).
465 Composite analysis of the effects of enso events on antarctica. *Journal of Climate*,
466 *29*(5), 1797–1808.
- 467 Wille, J. D., Favier, V., Dufour, A., Gorodetskaya, I. V., Turner, J., Agosta, C., & Co-
468 dron, F. (2019). West antarctic surface melt triggered by atmospheric rivers. *Nature*
469 *Geoscience*, *12*(11), 911–916.
- 470 Zhang, B., Yao, Y., Liu, L., & Yang, Y. (2021). Interannual ice mass variations over the
471 antarctic ice sheet from 2003 to 2017 were linked to el niño-southern oscillation. *Earth*
472 *and Planetary Science Letters*, *560*, 116796.
- 473 Zhu, Y., & Newell, R. E. (1998). A proposed algorithm for moisture fluxes from atmospheric
474 rivers. *Monthly weather review*, *126*(3), 725–735.
- 475 Zwally, H. J., Robbins, J. W., & Luthcke, S. B. (2017). Mass balance of east antarctic ice
476 sheet: Reconciling icesat altimetry with grace gravimetry and long-term ice history.
477 In *Agu fall meeting abstracts* (Vol. 2017, pp. C23D–08).